Journal for ImmunoTherapy of Cancer

Targeting tumor vasculature to improve antitumor activity of T cells armed ex vivo with T cell engaging bispecific antibody

Jeong A Park ,[1,2] Madelyn Espinosa-Cotton,[2] Hong-fen Guo,[2] Sebastien Monette,[3,4] Nai-Kong V Cheung [2]

To cite: Park JA, Espinosa-Cotton M, Guo H, *et al*. Targeting tumor vasculature to improve antitumor activity of T cells armed ex vivo with T cell engaging bispecific antibody. *Journal for ImmunoTherapy of Cancer* 2023;**11**:e006680. doi:10.1136/jitc-2023-006680

► Additional supplemental material is published online only. To view, please visit the journal online (http://dx.doi.org/10.1136/jitc-2023-006680).

Accepted 09 March 2023

[1]Pediatrics, Inha University Hospital, Incheon, Korea (the Republic of)
[2]Pediatrics, Memorial Sloan Kettering Cancer Center, New York, New York, USA
[3]Laboratory of Comparative Pathology, Memorial Sloan Kettering Cancer Center, New York, New York, USA
[4]Weill Cornell Medicine, New York, New York, USA

Correspondence to
Dr Nai-Kong V Cheung; cheungn@mskcc.org

ABSTRACT

Background Success of T cell immunotherapy hinges on the tumor microenvironment (TME), and abnormal tumor vasculature is a hallmark of most solid tumors and associated with immune evasion. The efficacy of T cell engaging bispecific antibody (BsAb) treatment relies on the successful trafficking and cytolytic activity of T cells in solid tumors. Normalization of tumor vasculature using vascular endothelial growth factor (VEGF) blockades could improve efficacy of BsAb-based T cell immunotherapy.

Methods Anti-human VEGF (bevacizumab, BVZ) or anti-mouse VEGFR2 antibody (DC101) was used as VEGF blockade, and ex vivo armed T cells (EATs) carrying anti-GD2, anti-HER2, or anti-glypican3 (GPC3) IgG-(L)-scFv platformed BsAb were used. BsAb-driven intratumoral T cell infiltration and in vivo antitumor response were evaluated using cancer cell line-derived xenografts (CDXs) or patient-derived xenografts (PDXs) carried out in BALB-*Rag2*$^{-/-}$IL-2R-γc-KO (BRG) mice. VEGF expression on human cancer cell lines was analyzed by flow cytometry, and VEGF levels in mouse serum were measured using VEGF Quantikine ELISA Kit. Tumor infiltrating lymphocytes (TILs) were evaluated using flow cytometry and by bioluminescence; both TILs and tumor vasculature were studied using immunohistochemistry.

Results VEGF expression on cancer cell lines increased with seeding density in vitro. BVZ significantly reduced serum VEGF levels in mice. BVZ or DC101 increased high endothelial venules (HEVs) in the TME and substantially enhanced (2.1–8.1 fold) BsAb-driven T cell infiltration into neuroblastoma and osteosarcoma xenografts, which was preferential for CD8(+) TILs versus CD4(+) TILs, leading to superior antitumor effects in multiple CDX and PDX tumor models without added toxicities.

Conclusions VEGF blockade using specific antibodies against VEGF or VEGFR2 increased HEVs in the TME and cytotoxic CD8(+) TILs, significantly improving the therapeutic efficacy of EAT strategies in preclinical models, supporting the clinical investigation of VEGF blockades to further enhance BsAb-based T cell immunotherapies.

WHAT IS ALREADY KNOWN ON THIS TOPIC

⇒ T-BsAbs built on the IgG-(L)-scFv platform were effective in driving T cells into solid tumors, inducing potent antitumor effects.

WHAT THIS STUDY ADDS

⇒ Targeting vascular endothelial growth factor (VEGF) by neutralizing VEGF or blocking VEGFR2 induced high endothelial venule formation in tumors, increasing the quantity of tumor infiltrating lymphocytes and their persistence, enabling effective dispersion of T cells, and enhancing antitumor effect.

HOW THIS STUDY MIGHT AFFECT RESEARCH, PRACTICE OR POLICY

⇒ This study supports the clinical investigation of VEGF blockades to further enhance BsAb-based T cell immunotherapies.

INTRODUCTION

T cell immunotherapy has proven efficacy against refractory or relapsed cancers. Despite the potent cytotoxicity, T cells often fail to penetrate deep into solid tumors, or even after successful infiltration they fail to fully function because of the immunosuppressive and hypoxic tumor microenvironment (TME).[1–4] An immature and chaotic tumor microvasculature is another challenge for T cell immunotherapy responsible for the hypoxic TME,[5] which alters tumor and immune cell metabolism, in turn promoting stromal desmoplasia and inflammation, contributing to therapeutic resistance and tumor progression.[6–8] Inhibiting abnormal tumor angiogenesis was first proposed as a therapeutic strategy by Folkman.[9] Targeting the abnormal microvasculature to improve tissue perfusion has the potential to overcome the immune-hostile TME by alleviating intratumoral hypoxia and converting immunosuppressive tumor infiltrating myeloid cells (TIMs) to immunosupportive ones, thereby improving antitumor response of T cell immunotherapy.[10 11]

Reciprocal interactions between endothelial and mesenchymal cells control the process of angiogenesis where the vascular endothelial growth factor (VEGF-A, in short as VEGF) and its receptors play pivotal roles.[12] VEGF is expressed at high levels in

many different types of cancer,[13] and tumor-derived VEGF stimulates tumor progression by inducing blood vessel formation, supporting immunosuppressive TIMs, and promoting T cell exhaustion by an autonomous VEGF and VEGFR2 feed-forward loop.[14] VEGF is a member of the homodimeric cysteine knot protein family growth factor[15] with affinity for the two tyrosine kinase receptors VEGFR1 (Flt-1) and VEGFR2 (KDR), with the latter functioning as the main receptor mediating most of the endothelial cell action.[16 17] Excessive activation of VEGFR2 mediates tissue-damaging vascular changes as well as the induction of tumor blood vessel expansion to support tumor growth. Unlike in normal vascular development and wound healing, VEGF expression is highly deregulated in primary and metastatic tumors, leading to endothelial cell hyperproliferation and loss of guidance on angiogenic sprouting that result in a chaotic tumor vascular bed.[12] VEGF is expressed by a variety of cells inside tumors, including the cancer cells, myeloid cells, stromal cells, and endothelial cells, reducing the ability of antigen-presenting cells (APCs) to prime T cells and causing systemic immunosuppression and immune effector cell anergy.[18]

Despite initial enthusiasm, anti-VEGF therapy alone including neutralizing antibodies, small molecular tyrosine kinase inhibitors, VEGF decoy receptors, and VEGF targeting ribozymes did not sufficiently improve survival when employed as alternatives to conventional anticancer treatments.[19] Subsequently when combined with chemotherapeutic agents or radiation treatment, these anti-VEGF therapies have shown more encouraging benefits. The US FDA first gave approval to bevacizumab (BVZ) as first-line therapy in combination with chemotherapeutic agents for metastatic colorectal carcinoma, non-squamous non-small cell lung cancer, ovarian carcinoma, breast cancer, renal cell carcinoma, and hepatocellular carcinoma.[20] In addition, recent studies reported synergistic effects of antiangiogenic agents and immune checkpoint inhibitors (ICIs) against advanced renal cell carcinoma and hepatocellular carcinoma.[21 22] However, many challenges remain. The potential role of anti-VEGF therapy in other solid tumors remains to be proven, and its impact on BsAb-based or CAR-based T cell immunotherapies has yet to be studied in depth. Here, we explore how VEGF blockades could affect BsAb-driven T cell infiltration into TME and how they potentiate antitumor effect of BsAb and T cell therapy in solid tumors.

METHODS

Tumor cell lines

Representative melanoma cell line M14 (NCI-DTP Cat# M14, RRID:CVCL_1395), small cell lung cancer cell line NCI-N87 (ATCC Cat# CRL-5822, RRID:CVCL_1603), human leukemia cell line HL6 (ATCC Cat# CCL-240, RRID:CVCL_0002), breast cancer cell line HCC1954 (ATCC Cat# CRL-2338, RRID:CVCL_1259), osteosarcoma cell line 143B (ATCC Cat# CRL-8303, RRID:CVCL_2270), and hepatoblastoma cell line Hep-G2 (ATCC Cat# HB-8065, RRID:CVCL_0027) were purchased. All the cell lines used were authenticated by short tandem repeat profiling with PowerPlex V.1.2 System (Promega), and periodically tested for mycoplasma infection using MycoAlert PLUS Mycoplasma Detection Kit (Lonza). The cells were cultured in RPMI1640 (Sigma) supplemented with 10% heat-inactivated fetal bovine serum (Life Technologies) at 37°C in a 5% CO_2 humidified incubator. The luciferase-labeled melanoma cell line M14Luc was generated by retroviral infection with an SFG-GF Luc vector.

Antibodies

To target VEGF, the anti-human VEGF (hVEGF) monoclonal IgG1 antibody BVZ (Avastin; Genentech, South San Francisco, CA) and anti-mouse VEGFR2 (mVEGFR2) antibody DC101 (Bio X Cell Cat# BE0060, RRID:AB_1107766) were used in vivo. The VEGF inhibitors were given intraperitoneally (ip) 1 day before each EAT injection. T cells armed ex vivo with BsAb (EATs) were generated as previously described.[23 24] Anti-GD2, anti-HER2, and anti-glypican3 (GPC3) BsAbs were mainly used in the experiments to test the synergy between EATs and VEGF blockades. These BsAbs were built on the IgG-(L)-scFv format using the sequences of anti-CD3 (huOKT3) IgG and anti-GD2 hu3F8 IgG1, anti-epidermal growth factor receptor-2 (HER2) (trastuzumab) IgG1, or anti-GPC3 antibody (clone GC33).[25 26] For each BsAb, scFv of huOKT3 was fused to the C-terminus of the light chain of human IgG1 via a C-terminal $(G_4S)_3$ linker.[27] N297A and K322A mutations on the Fc portion were generated with site-directed mutagenesis via primer extension in polymerase chain reactions.[28] The nucleotide sequence encoding each BsAb was synthesized by GenScript and was subcloned into a mammalian expression vector. BsAb was produced using Expi293 expression system (Thermo Fisher Scientific) separately. Antibodies were purified with protein A affinity column chromatography. The purity of these antibodies was tested by size-exclusion high-performance liquid chromatography as previously described.[23 24]

T cell expansion ex vivo

Serially expanded T cells from a single donor were used for each individual experiment. Peripheral blood mononuclear cells (PBMCs) were separated from buffy coats (New York Blood Center) using Ficoll. Naïve T cells were purified using Pan T cell isolation kit (Miltenyi Biotec, Cat#130096535) and expanded by CD3/CD28 Dynabeads (GibcoTM, Cat#11 132D) for 7 to 14 days in the presence of 30 IU/mL of IL-2. Expanded T cells were analyzed for their proportion of CD3(+), CD4(+), and CD8(+) T cells, and the fraction of CD4(+) or CD8(+) T cells was allowed between 40% and 60% to maintain consistency. Unless stated otherwise, these activated T cells were used for all T cell experiments.

Flow cytometry analysis of VEGF expression

Increasing numbers of various cancer cells (4×10^3 to 1×10^6 cells/well), including gastric cancer cell line NCI-N87, melanoma cell line M14Luc, leukemia cell line HL60, and breast cancer cell line HCC1954, were incubated in 96-well plates at 37°C in a 5% CO_2 humidified incubator. Cancer cells were harvested after 48 hours and stained with anti-hVEGF APC-conjugated antibody (R and D Systems Cat# IC2931A, RRID:AB_357310) according to manufacturer's instructions. 1×10^6 cancer cells were incubated with the antibody at 4°C for 30 min, washed, and analyzed by flow cytometry (BD FACS Calibur instrument and Attune NxT Flow Cytometer). Palivizumab was used as a control antibody. Data were analyzed with FlowJo V.10 software (FlowJo, RRID:SCR_008520).

Measurement of serum VEGF levels

Serum VEGF levels in murine plasma were measured using human VEGF Quantikine ELISA kit (R and D Systems Cat# DVE00, RRID:AB_2800364) according to the manufacturer's instruction. The intensity of the reaction was then revealed with tetramethylbenzidine and optical density was measured at 450 nm and at 540 nm using a Vmax microplate reader and Soft MAX Pro software (Molecular Devices, Menlo Park, California, USA). All samples were run in triplicate, and a standard curve was established for each assay.

Therapeutic study with mouse xenograft model

Cancer cell line xenografts (CDXs) were established using 1×10^6 143B and 5×10^6 Hep-G2 cells. Patient-derived xenografts (PDXs) were established from fresh surgical specimens with MSKCC IRB approval from patients diagnosed with neuroblastoma or osteosarcoma. Tumor cells in Matrigel (Corning Corp) were implanted subcutaneously on the right flank of each mouse. To avoid biological variables, only female mice were used for in vivo experiments. Treatment was initiated after tumors were established, average tumor volume of 100 mm^3 when measured using TM900 scanner (Piera, Brussels, Belgium). Before treatment, mice with small tumors (<50 mm^3) or mice with signs of skin infection were excluded from randomization to experimental groups. For ex vivo arming of T cells, a 10 µg of each BsAb was used to arm 2×10^7 T cells per injection.[23 24] BVZ or DC101 were given at 100 µg/dose intraperitoneally (ip) 1 day before each EAT injection. Tumor growth curves and overall survival were analyzed, and the overall survival was defined as the time from start of treatment to when tumor volume reached 2000 mm^3. To define the well-being of mice, complete blood cell counts (CBC) analyses, changes in body weight, behavior and physical appearance were closely monitored. All animal experiments were repeated twice more with different donor's T cells to ensure that our results were reliable.

T cell transduction

To obtain luciferase-expressing T cells (Luc(+) T cells), T cells isolated from peripheral blood were stimulated with Dynabeads Human T-Activator CD3/CD28 for 24 hours and then transduced with retroviral constructs containing tdTomato and click beetle red luciferase in RetroNectin-coated six-well plates in the presence of IL-2 (100 IU/mL) and protamine sulfate (4 µg/mL). Transduced T cells were cultured for 8 days before being used in animal experiments.

Bioluminescence imaging

Mice were anesthetized and imaged after intravenous injection of 3 mg of D-luciferin (Gold Biotechnology) on different days post T cell injection. Images were acquired using IVIS Spectrum CT In Vivo Imaging System (Caliper Life Sciences). Bioluminescence images were overlaid with photographs, regions of interest (ROI) were drawn based on the location and contour of the tumors, and total photon counts (photons/s) were obtained using Living image V.2.60 (Xenogen). Bioluminescence signal (total flux, photon/s) of tumor in the untreated group were used as baselines.

Immunohistochemistry and immunofluorescence staining

Immunohistochemistry (IHC) staining was performed at the MSK Molecular Cytology Core Facility using Discovery XT processor (Ventana Medical Systems) as previously described.[24 25] Tumor samples were fixed and embedded in paraffin. Anti-human CD45 (Abcam Cat# ab10558, RRID:AB_442810), anti-human CD3 (Agilent, Cat# A0452, RRID:AB_2335677), anti-human CD4 (Ventana Medical Systems Cat# 790-4423, RRID:AB_2335982), anti-human CD8 (Ventana Medical Systems Cat# 790-4460, RRID:AB_2335985), and anti-mouse CD31(Abcam Cat# ab134168, RRID:AB_2890012) were used, followed by a biotinylated secondary antibody. The detection was performed using a DAB detection kit (Ventana Medical Systems) or Alexa Fluor 488 or 568 Tyramide Reagent (Invitrogen). IHC staining of peripheral node addressin (PNA) (MECA79) was done with a manual protocol at Laboratory of Comparative Pathology using anti-PNA antibody (MECA79R) (Novus Cat# NBP2-78792). Immunofluorescence (IF) double staining of PNA and human CD3 was performed with the identical anti-PNA antibody and monoclonal rabbit anti-human CD3 antibody (clone MRQ-39, LS-C202826). Microscopic images were captured from tumor sections using a Nikon ECLIPSE Ni-U microscope and NIS-Elements V.4.0 imaging software. Antigen positive cells were counted with Qupath V.0.1.2 or using positive pixel count analysis.

Positive pixel count analysis

IHC slides were scanned (Aperio ScanScope XT) and analyzed by comparing positive pixel counts (Aperio Technologies). For analyzing tumor infiltrating lymphocytes (TILs), the largest area of intact tumor tissue was included, and oblique sections were avoided. Each slide was visually inspected to ensure specificity and sensitivity of antibody staining. After positive pixel count analysis was run, analyzed slides were examined to confirm that

positively identified pixels were consistent with lymphocyte or endothelial cell staining and not background staining. Percentages were calculated as the total number of positive pixels divided by the total number of pixels (% positive pixels/total pixels).

Flow cytometry analysis

For flow cytometry analyses of blood and tumor samples from mice, the following antibodies were used: anti-human CD45-APC (HI30, Speed BioSystems Cat# ZYF1027, RRID:AB_11160221), anti-human CD3-Percp/Cy5.5 (SK7, BioLegend Cat# 344808, RRID:AB_10640736), anti-human CD8-FITC (HIT8a, BioLegend Cat# 300906, RRID:AB_314110), anti-human CD4-PE/Cy7 (SK3, BioLegend Cat# 344612, RRID:AB_2028479), anti-mouse CD45-Brilliant Violet 711 (30-F11, BioLegend Cat# 103147, RRID:AB_2564383), anti-mouse CD11b-Brilliant Violet 570 (M1/70, BioLegend Cat# 101233, RRID:AB_10896949), anti-mouse Ly6G-FITC (1A8, BioLegend Cat# 127606, RRID:AB_1236494), anti-mouse Ly6C-PerCP/Cy5.5 (HK1.4, BioLegend Cat# 128012, RR:AB_1659241), and anti-mouse F4/80-PE (BM8, BioLegend Cat# 123110, RRID:AB_893486).

Cytokine release assays

EAT-induced human cytokine release was analyzed in vitro and in vivo. Human Th1 cell released cytokines were analyzed by LEGENDplexTM Human Th1 Panel (Biolegend, Cat# 741035). Five T cell cytokines including IL-2, IL-6, IL-10, IFN-γ and TNF-α were analyzed using mouse serum after treatment with EATs with or without VEGF blockade.

Statistical analysis

In vivo antitumor effect was compared by tumor growth curves and survival curves. Area under curves (AUCs) of tumor growth were calculated and compared among groups. Differences between groups indicated in the figures were tested for statistical significance by two-tailed Student's t-test for two sets of data while one-way analysis of variance with Tukey's post hoc test was used to compare data among three or more groups. All statistical analyses were performed by using GraphPad Prism V.8.0 for Windows (GraphPad Software, La Jolla, California, USA, www. graphpad. com). A $p<0.05$ was considered statistically significant. Asterisks indicate that the experimental p value is statistically significantly different from the associated controls at *p<0.05; **p<0.01; ***p<0.001; ****p<0.0001.

RESULTS

VEGF expression on tumor cells was positively correlated with seeding density in vitro

Flow cytometry revealed that VEGF expression on tumor cells increased when the cells were seeded more densely (online supplemental figure S1A). M14Luc, HCC1954, NCI-N87, and HL60 cells incubated at higher densities ($0.5–1 \times 10^6$ cells/well) had 2–10 fold higher MFIs than the cells seeded at the lowest density (4×10^3 cells/well). Particularly, M14Luc cells incubated at high density expressed significantly elevated levels of VEGF, while those incubated at low density did not express VEGF. The frequency of VEGF positivity also increased with cell density. While a few cancer cells expressed VEGF when incubated at the lowest density, more than 50% of cancer cells expressed VEGF at the highest cell density.

Anti-VEGF antibody reduced serum VEGF levels

Mice-bearing HGSOC1 osteosarcoma PDX were treated with T cells armed ex vivo with anti-HER2-BsAb (HER2-EATs) with or without VEGF blockade using BVZ (anti-hVEGF) or DC101 (anti-mVEGFR2). These antibodies have no known species cross reactivity (online supplemental table S1).[29–32] After two doses of each treatment (day 5 post-treatment, at 48 hours after second dose of BVZ or DC101), serum hVEGF levels were measured using Quantikine ELISA assay. In contrast to DC101 which had no effect on the level of h-VEGF in the mouse blood, BVZ significantly reduced serum hVEGF levels (online supplemental figure S1B).

Effect of VEGF blockade on cytokine levels after EAT therapy

To investigate the effect of VEGF blockade on cytokine release by T cells, we measured TH1 cell cytokines after injection of GD2-EATs following treatment with BVZ or DC101 in mice bearing neuroblastoma PDX (online supplemental figure S2A). The TH1 cell cytokines (IL-2, IL-10, IFN-γ, and TNF-α) were significantly lower in the BVZ combination group, but not in the DC101 combination group when analyzed 2 hours after the first dose of GD2-EATs. Thereafter, despite repeated injections of GD2-EATs, TH1 cell cytokines decreased overtime. IFN-γ, however, leveled off after day 7 and then rapidly rose between days 21 and 40 in both GD2-EATs plus VEGF blockade groups in contrast with other TH1 cytokines showing low levels (online supplemental figure S2B).

VEGF blockade facilitates BsAb-driven T cell trafficking into tumors when assayed by bioluminescence

We next studied the effect of VEGF blockade on BsAb-driven T cell trafficking into solid tumors. Luciferase transduced T cells armed with anti-HER2-BsAb (Luc (+) HER2-EATs) were administered in combination with BVZ or with DC101 to mice bearing HGSOC1 osteosarcoma PDX (figure 1A). The bioluminescence of TILs was monitored over time and quantified as a bioluminescence intensity (BLI). HER2-EATs successfully trafficked into tumors, where their bioluminescence peaked around day 5. Both BVZ and DC101 significantly increased the BLI of TILs in tumors. The duration of HER2-EAT persistence was also significantly longer with VEGF blockade; the AUC of BLI was much greater in VEGF blockade combination groups than those in HER2-EATs without VEGF blockade (7.5-fold (+ BVZ) and 2.4-fold (+DC101) increase in BLI AUC, p value of 0.05 and 0.016, respectively) (online supplemental

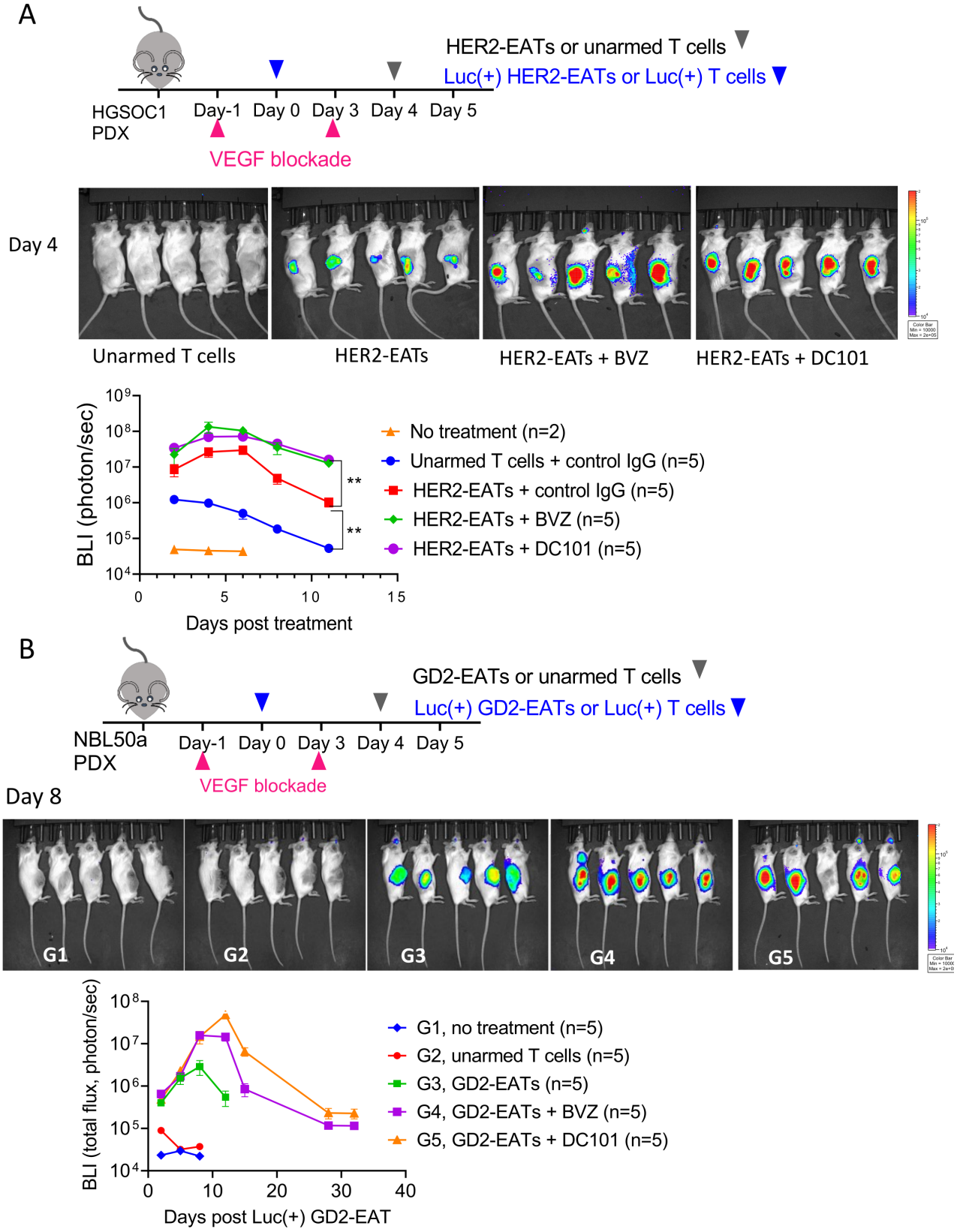

Figure 1 VEGF blockade enhances BsAb-driven T cell trafficking and persistence in tumors. (A) Luciferase transduced T cells armed ex vivo with anti-HER2 BsAb (Luc(+) HER2-EATs) were administered with BVZ or DC101 to mice bearing HER2(+) HGSOC1 osteosarcoma PDXs, and the bioluminescence of T cells in tumors was monitored over time and quantified as a bioluminescence intensity (BLI, photons/sec). (B) Luciferase transduced T cells armed ex vivo with anti-GD2 BsAb (Luc(+) GD2-EATs) were administered with BVZ or DC101 to treat GD2(+) neuroblastoma PDXs, and the bioluminescence of T cells in tumors was analyzed.*p<0.05; **p<0.01; ***p<0.001; ****p<0.0001. BsAb, bispecific antibody; BVZ, bevacizumab; EATs, T cells armed ex vivo with BsAb; PDXs, patient-derived xenografts; VEGF, vascular endothelial growth factor.

table S2). The effect of VEGF blockade on BsAb-driven T cell trafficking was tested in a separate tumor model using GD-EATs against a GD2 positive neuroblastoma PDX (figure 1B). Both BVZ and DC101 increased BLI in tumors (2.8-fold and 8.1-fold increase in BLI-AUC, p value 0.01 and 0.05, respectively), significantly prolonging TIL persistence. The TIL bioluminescence peaked around days 7–14 and remained detectable more than 30 days post-treatment. Online supplemental figure S3 exhibits prolonged bioluminescence persistence in combination groups.

VEGF blockade significantly increased T cell infiltration into tumors when assayed by immunostaining

To study the effect of VEGF blockade on T cell infiltration into tumors, 143B osteosarcoma CDXs were analyzed on day 60 post-treatment (online supplemental figure S4A). While osteosarcoma CDXs treated with unarmed T cells had few hCD45(+) TILs irrespective of VEGF blockade, tumors treated with GD2-EATs had higher TILs on day 60 post-treatment, and, in the presence of BVZ or DC101, not just hCD45(+) TILs but also hCD8(+) TILs were significantly increased. This effect of VEGF blockade was confirmed by IHC staining. In contrast to tumors treated with unarmed T cells with or without VEGF blockade which had few TILs, osteosarcoma CDXs treated with GD2-EATs showed diffuse T cell infiltration (online supplemental figure S4B). TILs were significantly increased in both BVZ and DC101 combination-treated groups compared with the group treated with GD2-EATs alone ($p<0.0001$ and $p<0.0001$, respectively). There was no difference between the two blocking antibodies ($p=0.69$).

The enhanced intratumoral T cell infiltration with VEGF blockade was reproduced in a second model where neuroblastoma PDXs were treated with GD2-EATs with or without VEGF blockade. Tumors were harvested on day 10 post-treatment and analyzed by flow cytometry (figure 2A). Tumors treated with GD2-EATs showed higher frequencies of intratumoral hCD45(+) T cells than tumors treated with unarmed T cells as reported previously.[23 33] When BVZ or DC101 was combined with GD2-EATs, the increase in hCD45(+) TILs was much more pronounced. We also compared CD3(+), CD4(+), and CD8(+) T cell infiltration by IHC staining (figure 2B). VEGF blockade significantly increased TILs in tumors treated with GD2-EATs. The addition of BVZ or DC101 led to a 3-fold and 2.5-fold increase of CD3(+) TILs, respectively, compared with those treated with GD2-EATs alone. While CD4(+) TILs increased only 1.1-fold and 1.3-fold, respectively, without significant difference between GD2-EATs group, CD8(+) TIL increase was more robust, at 5-fold and 4-fold, respectively. Because of these shifts, the CD8/CD4 ratio significantly increased when VEGF blockade was combined with GD2-EATs (figure 2C and table 1).

VEGF blockade and TIM cells

To test if VEGF blockade affected CBC or frequency of TIM cells, CBC and flow cytometry analysis of tumors were performed on day 5 and day 10 post-EAT treatment, respectively. There were no significant changes in the red blood cell, leukocyte, or platelet counts (online supplemental figure S5A). The effect on TIMs was also analyzed using flow cytometry performed on tumors (online supplemental figure S5B). As reported previously, while tumors in the no treatment (G1) or unarmed T cells (G2) groups had fewer TIMs, tumors treated with GD2-EATs (G3) had abundant mCD45(+) mCD11b(+) TIMs.[33] When we compared VEGF blockade combination groups (G4, GD2-EATs plus BVZ, and G5, GD2-EATs plus DC101), there was no significant difference in the frequencies of TIMs between G4 and G5, either among the $Ly6G^{+}$ PMN-MDSC, $Ly6C^{hi}$ M-MDSC, $F4/80^{+}$ TAM, or $Ly6C^{lo}$ MDSC subsets. We repeated TIM analysis in a different tumor model using 143B CDXs where blood and tumors were analyzed on day 5 and day 60 post-treatment, respectively. Again, VEGF blockade did not result in significant differences in CBC among groups (online supplemental figure S6A), and there were no differences in TIM frequencies including PMN-MDSC, M-MDSC, and TAM subsets among groups with or without VEGF blockade (online supplemental figure S6B).

Effect of VEGF blockades on intratumoral microvasculization

Intratumoral blood vessels in neuroblastoma PDXs were stained with anti-mCD31 antibody to study the effect of VEGF blockade on tumor microvasculature (figure 3A). Although there was no difference among three groups without VEGF blockade (no treatment (G1), unarmed T cells (G2), and GD2-EATs (G3)), there was a significant increase in mCD31(+) endothelial cell staining in VEGF blockade combination groups (G3 vs G4 (+BVZ), $p=0.0062$; G3 vs G5 (+DC101), $p=0.0038$) on day 10 post-treatment. Notably, VEGF blockade changed the shape of intratumoral blood vessels (figure 3B), which appeared thickened with plump cuboidal endothelial cells characteristic of high endothelial venules (HEVs),[34 35] contrasting with the vessels in other groups without VEGF blockade (G1, G2, and G3) which appeared as flat and thin endothelial cells typical of tumor microvasculature. Indeed, the endothelial cells in tumors treated with VEGF blockade exhibited positive IHC staining for PNA/MECA79, a specific marker for HEVs[34] (figure 3C). PNA/MECA79 and hCD3 double IF staining also showed T cell infiltration around the HEVs (figure 3D). Table 2 analyzes the distribution of tumor-associated HEVs (TA-HEVs) and hCD3(+) TILs and compared their densities among groups. The tumors treated with GD2-EATs plus BVZ or DC101 showed much higher densities of HEVs (number of PNA/MECA79(+) vessels per tumor area) compared with those in GD2-EATs alone. The density hCD3(+) TILs (hCD3(+) T cells per tumor area) was correlated with the density of HEVs: the tumors treated with GD2-EATs plus BVZ or DC101 showed higher densities of hCD3(+) TILs. When we compared the ratio of hCD3(+) TIL density in peri-HEVs 50 µm (the tumor region located within a 50 µm radius around HEVs) to the hCD3(+) TIL density

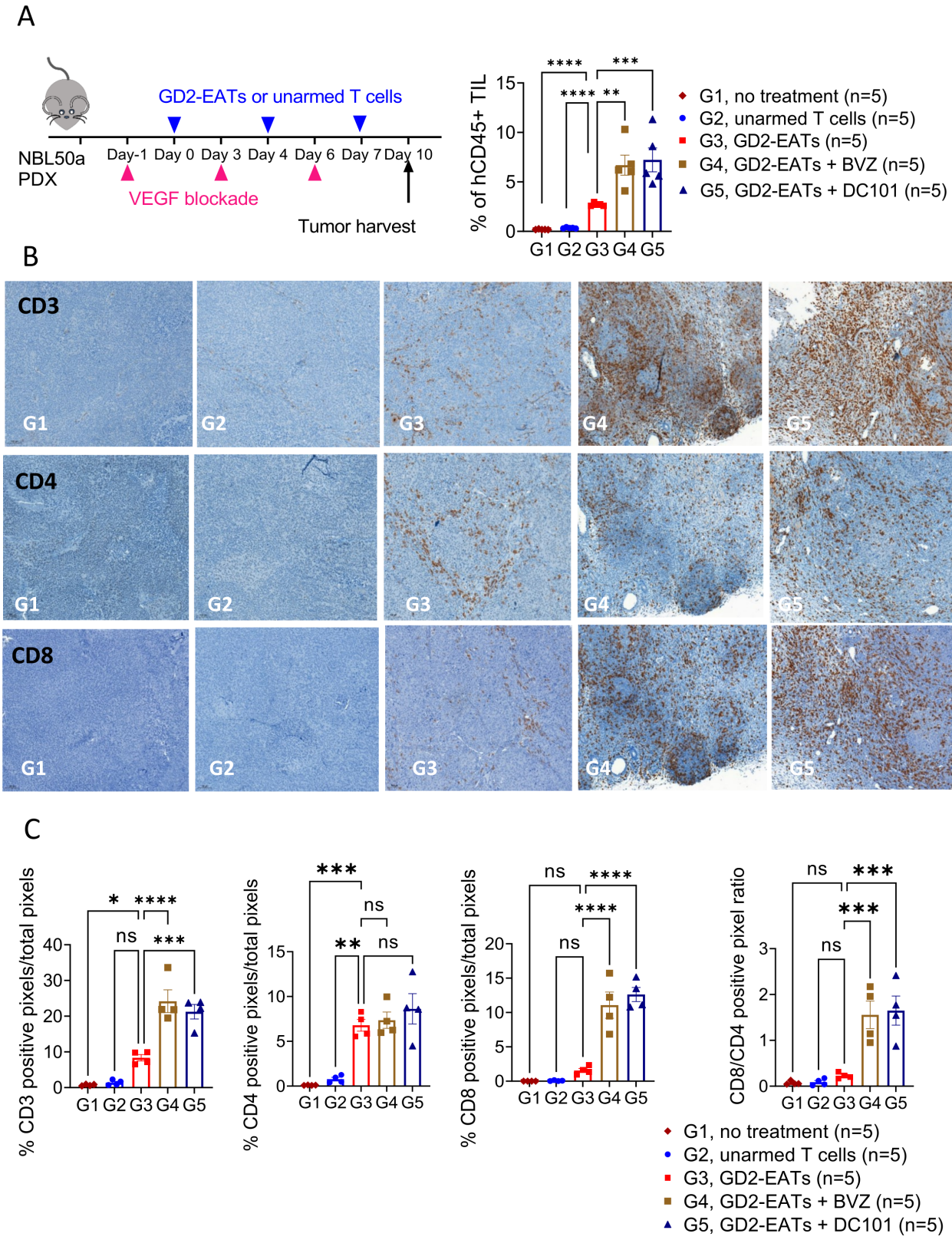

Figure 2 VEGF blockade enhances GD2-EAT infiltration into neuroblastoma and particularly, increased intratumoral CD8(+) T cells. (A) Neuroblastoma PDXs were treated with a combination of GD2-EATs and anti-VEGF (BVZ) or VEGFR2 antibody (DC101). Tumors were harvested on day 10 post-EAT treatment and analyzed by flow cytometry. (B) Immunohistochemical staining (IHC) of neuroblastoma PDXs. Tumors were harvested on day 10 post-EAT treatment and stained with anti-human CD3, anti-human CD4, and anti-human CD8 antibody. (C) Intratumoral CD3, CD4, and CD8 T cells were quantified by positive pixel count analyses and compared among groups. G1, no treatment; G2, unarmed T cells; G3, GD2-EATs; G4, GD2-EATs plus BVZ; G5, GD2-EATs plus DC101. *p<0.05; **p<0.01; ***p<0.001; ****p<0.0001. BVZ, bevacizumab; EATs, T cells armed ex vivo with BsAb; PDXs, patient-derived xenografts; VEGF, vascular endothelial growth factor.

Table 1 Distribution of CD3, CD4, and CD8 T cells in neuroblastoma patient-derived xenografts by positive pixel count analyses

Treatment	% CD3(+) cells (mean±SD)	P value (vs GD2-EATs)	% CD4(+) cells (mean±SD)	P value (vs GD2-EATs)	% CD8(+) cells (mean±SD)	P value (vs GD2-EATs)	Ratio of CD8 to CD4 T cells	P value (vs GD2-EATs)
Unarmed T cells	1.4±0.7	0.05	0.8±0.4	0.001	0.07±0.06	0.662	0.1±0.07	0.96
GD2-EATs	8.4±2	–	6.8±1.3	–	1.1±0.3	–	0.2±0.06	–
GD2-EATs+BVZ	24±6	<0.0001	7.4±1.8	0.98	5±3	<0.0001	1.6±0.6	0.001
GD2-EATs+DC101	21±4	<0.0001	8.6±3.4	0.45	4±4	<0.0001	1.7±0.6	0.001

BVZ, bevacizumab; EAT, T cell armed ex vivo with BsAb.

in the whole tumor area, VEGF blockade combination groups showed lower hCD3(+) T cell densities around peri-HEVs 50 µm than the group of GD2-EATs alone, consistent with a more effective dispersion of TILs after extravasation.

VEGF blockade improved tumor responsiveness to EAT therapy in vivo

Next, we studied the effect of VEGF blockade on in vivo antitumor response to EATs. We tested the effect in four different tumor models including two osteosarcomas, one neuroblastoma, and one hepatoblastoma. First, we treated osteosarcoma 143B CDXs with GD2-EATs plus BVZ or DC101 (figure 4A). BVZ or DC101 with unarmed T cells did not show any antitumor effect, and GD2-EATs without VEGF blockade showed only modest tumor suppression. When BVZ or DC101 was combined, the antitumor effect of GD2-EATs was profoundly improved (p=0.007 and p=0.0041, respectively), significantly prolonging mouse survival (p=0.0002). In the second tumor model, we treated TEOSC1 osteosarcoma PDXs with 2 doses of GD2-EATs and 3 doses of either BVZ or DC101 (figure 4B). VEGF blockade plus GD2-EATs produced long-term remission past 6 months, significantly longer than GD2-EATs alone (p=0.0221). Of particular interest were the histological changes among tumors treated by GD2-EATs plus VEGF blockade, showing fibrous and cavitary bone lesions characterized by extramedullary hematopoiesis and mineralization without visible tumor cells, in contrast to relapsed tumors in the GD2-EATs group showing chondroid differentiating osteosarcoma (figure 4C). In the third tumor model, we treated neuroblastoma PDXs with GD2-EATs in the presence of VEGF blockade. Contrary to the GD2-EATs alone group showing unabated tumor growth, GD2-EATs plus BVZ or plus DC101 presented significantly better antitumor effect in vivo (figure 5A). The combinations successfully ablated all tumors and demonstrated sustained remission without clinical toxicity, significantly prolonging survival (p<0.0001). In the fourth model, a HepG2 hepatoblastoma CDX was treated with T cells armed ex vivo with anti-glypican 3 BsAb (GPC3-EATs) with VEGF blockade (figure 5B). In contrast to unarmed T cells or GPC3-EATs plus control IgG, GPC3-EATs plus BVZ or DC101 significantly enhanced antitumor response, confirming the synergy between VEGF blockade and EATs.

DISCUSSION

T-BsAbs built on the IgG-(L)-scFv platform, whether administered as stand-alone or as carried on EATs are effective in driving T cells into solid tumors, inducing potent antitumor effects against a variety of human cancer targets.[22 28–30] These BsAbs transformed immunologically 'cold tumors' into 'hot tumors' by recruiting TILs, followed by TIMs.[33] We have previously shown that depleting TIMs including PMN-MDSCs, M-MDSCs, and TAMs could significantly enhance BsAb-driven T cell infiltration and persistence in tumors, resulting in boosted antitumor immune response against solid cancers.[33] Independent from these TIM depleting strategies, here we demonstrated that targeting VEGF by neutralizing the ligand or blocking the receptor could also significantly increase BsAb-driven T cell infiltration into solid tumors and enhance antitumor response without affecting blood cell count or immunosuppressive TIM frequencies. Although combination therapies of VEGF inhibitors and chemotherapy or ICIs have produced superior treatment outcomes compared with single treatment modalities,[20 36 37] synergy between VEGF blockade and BsAb or CAR T cells has not been fully investigated. In our preclinical models, the combination of EATs and VEGF blockade was tolerable without significant cytokine release while inducing long-term immune surveillance associated with delayed IFN-γ surge. Both VEGF blockades, neutralizing VEGF by BVZ or blocking VEGFR2 by DC101, induced HEV formation in tumors, increasing the quantity of TILs and their persistence, enabling effective dispersion of T cells, and enhancing antitumor effect.

The activation of VEGFR2 by VEGF is the most critical driver of tumor angiogenesis,[38] and therapeutic intervention aimed at inhibiting the VEGF and VEGFR2 pathway has become a mainstay of treatment for cancer. The VEGF/VEGFR2 signaling contributes to cancer cell resistance on multiple mechanisms. Activated VEGFR2 results in the activation of diverse downstream pathways (eg, selective catalytic reduction, phospholipase C-γ,

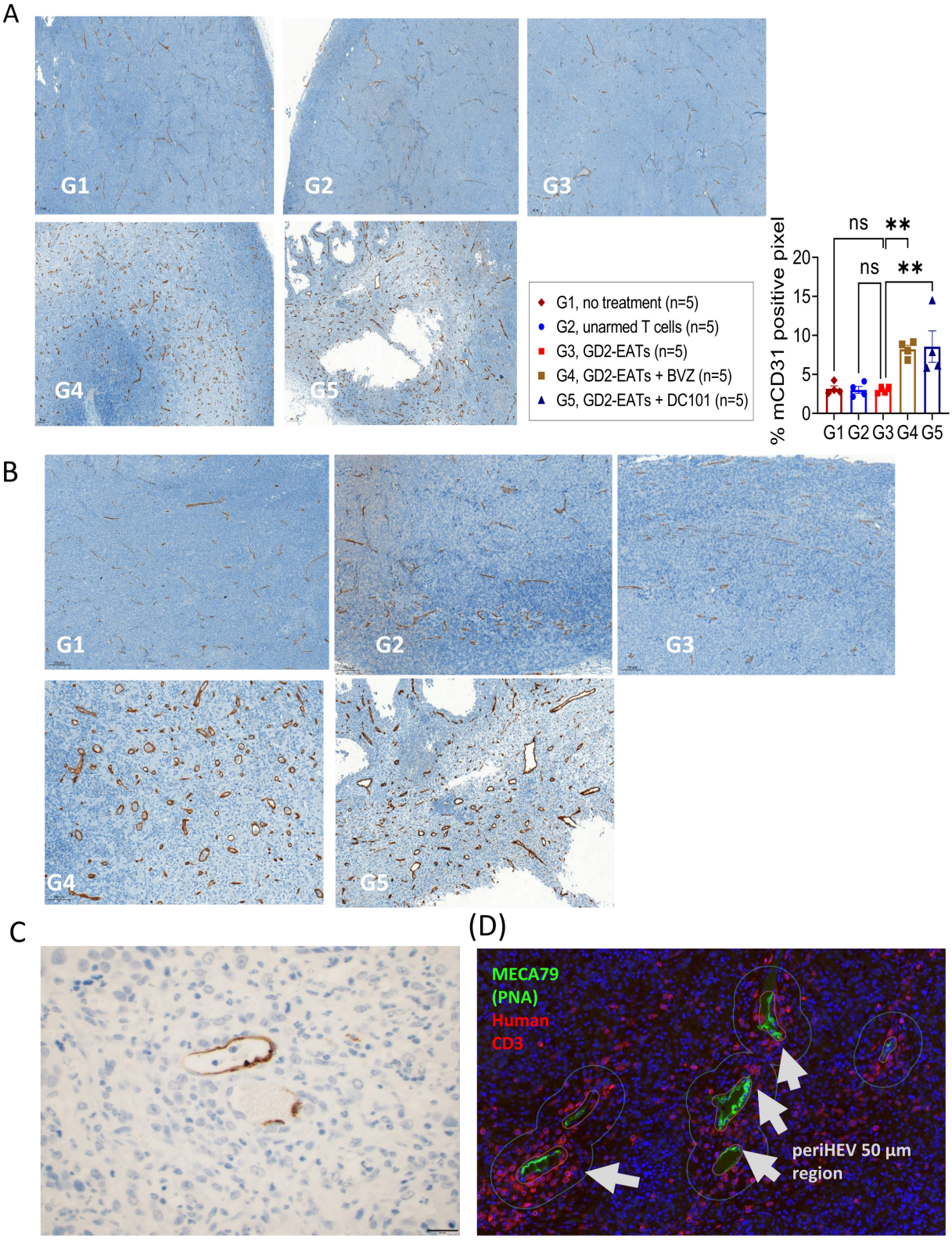

Figure 3 The effect of VEGF blockade on tumor microvasculature. (A) Neuroblastoma PDXs were harvested on day 10 post-EAT treatment, and intratumoral blood vessels were stained using anti-mouse CD31 antibody. CD31 positive cells were quantified with positive pixel count analysis. (B) Combinations of GD2-EATs and anti-VEGF (BVZ) (G4) or anti-VEGFR2 antibody (DC101) (G5) induced high endothelial venules (HEVs) in tumors. (C) Representative image of HEVs in a tumor from G4 (GD2-EATs+BVZ), positively stained with anti-peripheral node addressin (PNA)/MECA79 antibody which specifically stain HEVs and no other types of blood vessels. (D) Double immunofluorescence (IF) staining of PNA/MECA79 and human CD3 was performed in tumors from G4, displaying HEVs and T cell distribution around them. G1, no treatment; G2, unarmed T cells; G3, GD2-EATs; G4, GD2-EATs plus BVZ; G5, GD2-EATs plus DC101. *p<0.05; **p<0.01; ***p<0.001; ****p<0.0001. BVZ, bevacizumab; EATs, T cells armed ex vivo with BsAb; PDXs, patient-derived xenografts; VEGF, vascular endothelial growth factor.

Table 2 Distribution of tumor-associated high endothelial venules (TA-HEVs) and CD3(+) tumor infiltrating lymphocytes (TILs)

Group	Treatment	HEVs in tumor (no of PNA(+) vessels)	Density of HEVs (HEVs/ whole tumor area mm^2)	Density of hCD3(+) T cells (T cells/area mm^2)		Ratio of hCD3(+) TIL density in peri-HEV 50 µm to whole tumor area
G2	Unarmed T cells	0	0.0	Peri-HEV 50 µm	na	na
				Whole tumor	5	
G3	GD2-EATs	5	0.1	Peri-HEV 50 µm	4145	34.83
				Whole tumor	119	
G4	GD2-EATs+BVZ	21	0.5	Peri-HEV 50 µm	1747	12.04
				Whole tumor	145	
G5	GD2-EATs+DC101	14	0.4	Peri-HEV 50 µm	1149	9.38
				Whole tumor	123	

Peri-HEV 50 µm, the tumor region located within a 50 µm radius around HEVs.
BVZ, bevacizumab; EAT, T cell armed ex vivo with BsAb; na, not applicable.

phosphoinositide-3-kinase, P38 mitogen-activated protein kinase and focal adhesion kinase), culminating in specific changes in tumor microvasculature including endothelial cell shape, adhesion, permeability, survival, proliferation, vasodilatation, and migration.[39] The VEGFR2 signaling in tumor cells mediated by VEGF receptor tyrosine kinases (RTKs) and neuropilins potentiates the signaling function of growth factor RTKs and integrins crucial for cancer cell survival.[13] The VEGFR2 is also known to induce an immunosuppressive TME by recruiting neutrophils, MDSCs, and M2 TAMs, while inhibiting T cell proliferation and cytotoxicity with upregulating checkpoint inhibitors on cytotoxic CD8(+) T cells.[39]

In this study, the contribution of mVEGF released from mouse stroma and TIMs can be a major confounding factor in interpreting the pharmacological effects of VEGF blockades. Despite the sequence homology of near 85%–89% between human and murine VEGFs and VEGFR2s, species-specific antibodies such as BVZ and DC101 are available.[40 41] BVZ only inhibits the tumor-derived hVEGF and does not inhibit mVEGF, while DC101 does not react with hVEGFR2.[29 40 41] In our BRG mouse model, only tumor and T cells were human derived, and TME, including myeloid cells, vasculature and stroma, was all mouse derived, and we used BVZ to target hVEGF released from tumor cells and DC101 to target mVEGFR2 expressed on mouse endothelium or mouse-derived MDSCs. This study suggests an autocrine loop for hVEGF in tumor cell growth[14 42] and implies that mVEGF derived from the tumor stroma and TIMs could engage mVEGFR2 to produce the downstream effects. Although the action of hVEGF on mVEGFR2 is expected to be weak,[29 32] DC101 treatment is known to increase levels of plasma hVEGF in human tumor-bearing mice[30]; our data also suggest that hVEGF released by human tumors is active on both human and mouse VEGFR2, modulating murine endothelial cell formation in the TME. While BVZ neutralizes hVEGF signaling on both human and mouse cells, DC101 blockades only mVEGFR2 but not hVEGFR2, thereby pinpointing the importance of mouse angiogenic pathways. In our studies, hVEGF and mVEGF both contributed to tumor growth, since BVZ and DC101 independently improved tumor responsiveness to EAT therapy. Blockade of both tumor-derived and stroma-derived VEGF by cross-species VEGF blocking antibodies showed more potent tumor suppressing effect when compared with single blockade of tumor-derived VEGF by BVZ.[39] Future studies to explore these combined effects in BsAb-based T cell immunotherapy in preclinical models and in humans will be of interest.

One of the interesting findings is the HEV formation in tumors following treatment with GD2-EATs and BVZ or DC101. HEVs, specialized postcapillary venules, are the main sites of lymphocyte tethering, rolling, and sticking in the tumor microcirculation.[43–45] While typical tumor blood vessels overexpress endothelin B receptor inhibiting lymphocyte adhesion and infiltration into tumors, HEVs are known to express specific chemokines and adhesion molecules ICAM-1/ICAM-2 and VCAM-1, which contribute to the selective lymphocyte trafficking across these blood vessels.[46 47] HEVs express high levels of sulfated sialomucins recognized by the HEV-specific antibody MECA79 (PNA),[48] and the density of MECA79(+) TA-HEVs correlates with densities of CD3(+) and CD8(+) T cells and CD20(+) B cells, as well as with favorable clinical outcomes in breast cancer and melanoma.[47 49] Combinations of anti-angiogenic therapy and ICIs also induced HEV formation in breast and pancreatic cancers, improving the antitumor efficacy.[47 50 51] Another intriguing finding was the ratio of hCD3(+) TIL density in peri-HEVs 50 µm to whole tumor area. While the tumors treated with GD2-EATs plus BVZ or DC101 showed a much higher density of hCD3(+) TILs and HEVs than those in GD2-EATs alone, the T cells in VEGF blockade combination groups were more diffusely dispersed into tumors, contrasting to those in GD2-EATs monotherapy group showing that majority of CD3(+) T cells clustered around HEVs. Those findings suggest that VEGF blockade promotes TA-HEVs to increase exit points for T cells while at the same time increasing ability of TILs to disseminate

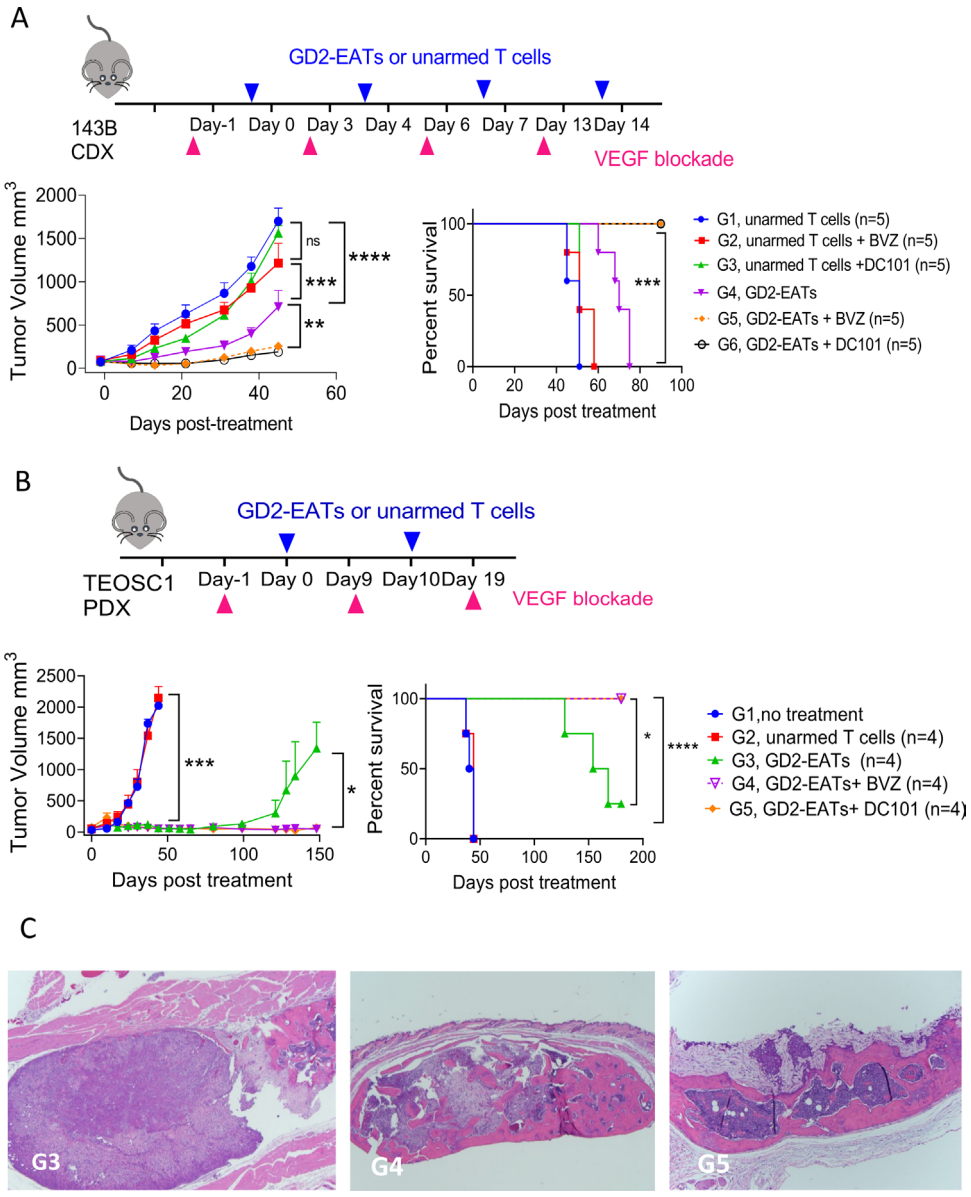

Figure 4 In vivo antitumor effect of combination therapies of GD2-EATs and VEGF blockades against osteosarcomas. (A) 143B osteosarcoma CDXs were treated by GD2-EATs with or without VEGF blockades, and in vivo tumor suppressing effects and overall survival were compared among groups. (B) TEOSC1 osteosarcoma PDXs were treated by GD2-EATs with or without VEGF blockade. Tumor growth curves and overall survival were plotted and compared among groups. G1, no treatment; G2, unarmed T cells; G3, GD2-EATs; G4, GD2-EATs plus BVZ; G5, GD2-EATs plus DC101. (C) H&E staining of tumors harvested on day 180 post-treatment. Tumors in G4 and G5 (combination therapy of GD2-EATs with VEGF blockade) showed extramedullary hematopoiesis and bone mineralization without visible tumor cells, which contrasted with those in G3 (GD2-EATs alone) showing viable chondroid differentiating osteosarcoma. *p<0.05; **p<0.01; ***p<0.001; ****p<0.0001. BVZ, bevacizumab; EATs, T cells armed ex vivo with BsAb; PDXs, patient-derived xenografts; VEGF, vascular endothelial growth factor.

into tumor parenchyma rather than clustering around HEVs, leading to more effective shrinkage of tumors. As shown in previous reports, VEGF blockade attenuates VEGF/VEGFR2-dependent angiogenesis, thereby reducing vascular cell proliferation, and increases HEVs in tumors, relieving hypoxia while normalizing tumor pH, thereby facilitating T cell dispersion after extravasation to maximize antitumor immune response.[50 52 53]

In addition, VEGF blockade significantly increased CD8 to CD4 TIL ratio. One of the mechanisms of regulating the tumor-endothelial barrier and T cell infiltration into tumors involves the selective expression of Fas ligand (FasL, CD95L) in the vasculature of human and mouse solid tumors but not in normal vasculature.[54] Tumor-derived VEGF, IL-10, and prostaglandin E2 (PGE2) cooperatively induced FasL expression in endothelial cells, which induces CD8(+) T cell apoptosis but not Tregs, resulting in scarce CD8(+) T cell infiltration and a predominance of FoxP3(+) Tregs.[54 55] Pharmacological inhibition of VEGF and PGE2 attenuated FasL expression and increased CD8(+) T cells over FoxP3(+) Tregs, inducing CD8(+) T cell-dependent tumor suppression.[56]

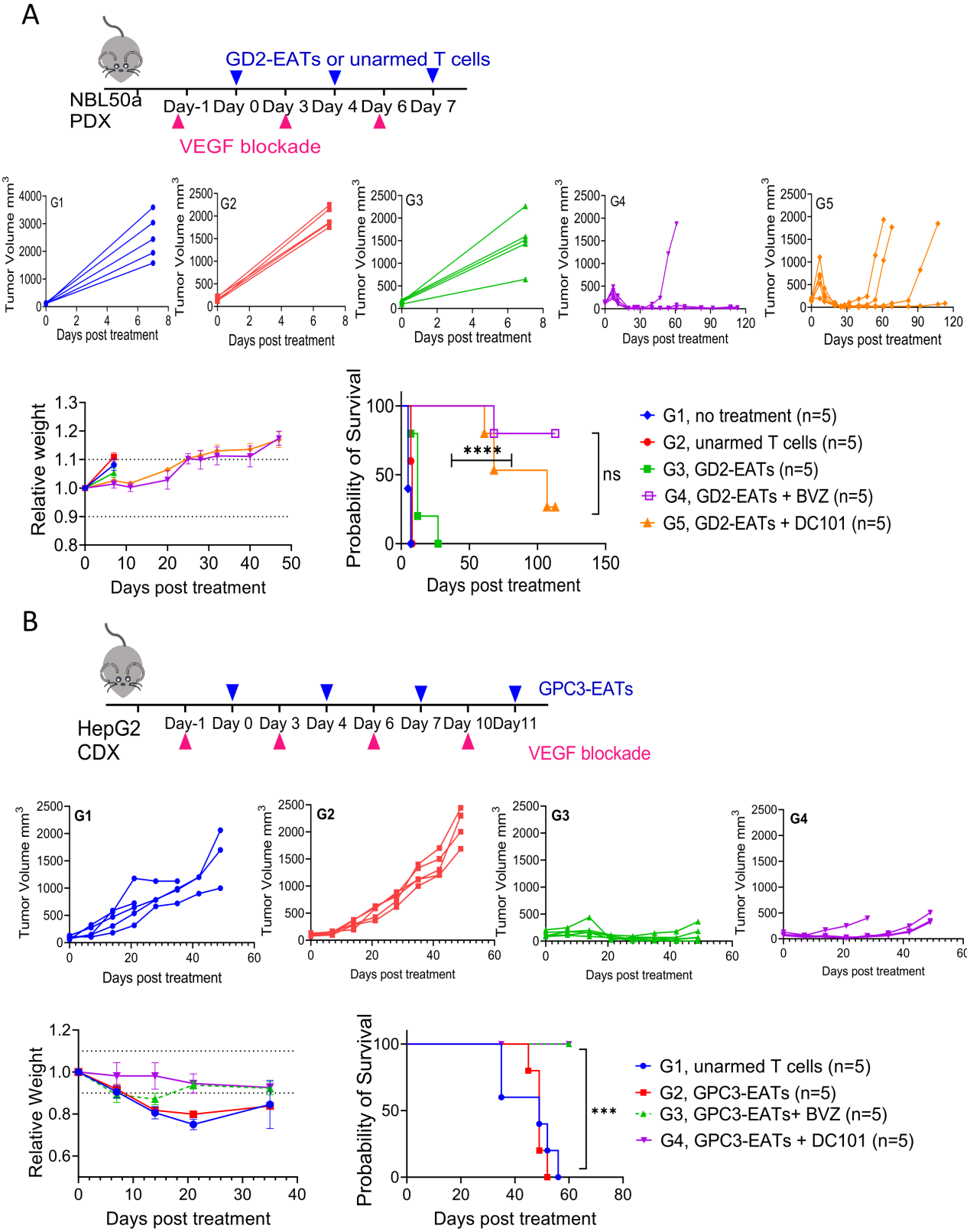

Figure 5 In vivo antitumor effect of combination therapies of EATs and VEGF blockade. (A) Synergistic antitumor effects between GD2-EATs and VEGF blockades were tested in a neuroblastoma PDX model. Tumor growth, mouse weight, and overall survival curves were plotted and compared among groups. G1, no treatment; G2, unarmed T cells; G3, GD2-EATs; G4, GD2-EATs plus BVZ; G5, GD2-EATs plus DC101. (B) In vivo antitumor effects of GPC3-EATs (T cells armed ex vivo with anti-GPC3 BsAb) and VEGF blockade combination were tested using HepG2 hepatoblastoma CDXs. Tumor growth, changes in body weight, and overall survival were monitored and analyzed. G1, unarmed T cells; G2, GPC3-EATs; G3, GPC3-EATs plus BVZ; G4, GPC3-EATs plus DC101. *p<0.05; **p<0.01; ***p<0.001; ****p<0.0001. BsAb, bispecific antibody; BVZ, bevacizumab; EATs, T cells armed ex vivo with BsAb; PDXs, patient-derived xenografts; VEGF, vascular endothelial growth factor.

Another notable finding of this study is the histology suggestive of differentiation following EAT therapy in the presence of VEGF blockade. Osteosarcoma PDXs treated with GD2-EATs in combination with BVZ or DC101 showed new bone formation at the tumor sites, supporting the role of VEGF signaling in osteoblastic maturation and mineralization.[57] VEGF secreted by tumor cells promotes dedifferentiation and endothelial-to-mesenchymal transition (EndMT), consequently promoting tumor growth and invasion, and it can facilitate the function of cancer stem cells, leading to treatment resistance.[13 58] Deletion of VEGFR2 in osteoblast precursors enhanced osteoblastic differentiation and mineralization during bone repair mainly through mechanisms of intramembranous ossification.[57] Neutralizing VEGF produced by osteosarcoma cells may enhance osteoblast differentiation and new bone formation at the tumor site while prohibiting EndMT, reducing production of cancer-associated fibroblasts.

We should note that this manuscript only showed the impact of anti-VEGF therapy on trafficking of preactivated and ex vivo expanded T cells, which may not directly apply to systemic therapy with BsAb where T cells are activated directly in vivo. In mice engrafted with fresh PBMCs without ex vivo activation, intravenous BsAb successfully drove CD3(+) T cells into tumors to exert potent antitumor effect as well.[24] However, by using PBMC, the effect of T cells could not be easily isolated.

In conclusion, our study demonstrated the therapeutic potential of VEGF blockade using anti-VEGF or anti-VEGFR2 antibody in combination with tumor-specific EATs. BVZ and DC101 significantly enhanced intratumoral EAT infiltration and persistence of CD8(+) T cells, improving in vivo antitumor immune response and survival. Our findings suggest that both VEGF and VEGFR2 represent attractive targets to improve the antitumor effect of T cell immunotherapy, most likely by vascular normalization and inducing HEVs, increasing CD8(+) T cell survival and dispersion, and mitigating the immunosuppressive TME. Future studies directed at exploring the signaling pathways that connect angiogenesis, hypoxia, metabolism, T cell activation, and exhaustion should yield further insights into how to best combine antiangiogenic therapy with BsAb-based T cell immunotherapy for patients with cancer.

Acknowledgements We would like to thank Dr. Hong Xu for providing the anti-HER2 BsAb and Dr. Zhihao Wu and See Liang Ng for anti-GPC3 BsAb. We also want to acknowledge Ms. Hoa Tran for helping animal experiments, Dr. Afsar Barlas for immunohistochemical staining of tumor sections, Mr. Eric Rosiek for positive pixel count analysis of IHC slides, and Drs. Adam Michel. and Ileana Miranda in the Laboratory of Comparative Pathology for reviewing pathology of the xenografts. We also thank Dr. Elisa De Stanchina for providing PDXs for these studies.

Contributors JAP and N-KVC designed and performed the experiments, interpreted and analyzed the results, and wrote the initial manuscript. Both revised this manuscript. ME-C coordinated the immunohistochemical analysis. HG prepared bispecific antibodies and supported experiments. SM reviewed the pathology of the xenografts and interpreted the data. All authors reviewed this manuscript and approved the final submitted version. JAP and N-KVC are responsible for the overall content as guarantor.

Funding This work was supported by funds from Enid A. Haupt Endowed Chair, the Robert Steel Foundation, Kids Walk for Kids with Cancer. Technical service provided by the MSK Animal Imaging Core Facility, Antitumor Assessment Core Facility, and Molecular Cytology Core Facility were supported in part by the NCI Cancer Center Support Grant P30 CA008748. This work was also supported by Inha University Research Fund and a grant of the Korea Health Technology R&D Project (grant number: HI12C1488).

Competing interests Both N-KVC and JAP were named as inventors on the patent of EATs filed by MSK. Both MSK and N-KVC have financial interest in Y-mAbs, Abpro-Labs and Eureka Therapeutics. N-KVC reports receiving past commercial research grants from Y-mabs Therapeutics and Abpro-Labs. N-KVC was named as inventor on multiple patents filed by MSK, including those licensed to Ymabs Therapeutics, Biotec Pharmacon, and Abpro-labs. N-KVC is a SAB member for Eureka Therapeutics.

Patient consent for publication Not applicable.

Ethics approval All animal procedures were performed according to Memorial Sloan Kettering Cancer Center's institutional Animal Care and Use Committee (IACUC) approved protocol (#09-05-10). BALB/c Rag2−/−IL-2Rγc−/− (BRG) mice purchased from Taconic were used in this study.

Provenance and peer review Not commissioned; externally peer reviewed.

Data availability statement All data relevant to the study are included in the article or uploaded as online supplemental information.

ORCID iDs
Jeong A Park http://orcid.org/0000-0003-3690-6747
Nai-Kong V Cheung http://orcid.org/0000-0001-6323-5171

REFERENCES

1 Polyak K, Haviv I, Campbell IG. Co-Evolution of tumor cells and their microenvironment. *Trends Genet* 2009;25:30–8.
2 Gabrilovich DI, Nagaraj S. Myeloid-Derived suppressor cells as regulators of the immune system. *Nat Rev Immunol* 2009;9:162–74.
3 Murdoch C, Muthana M, Coffelt SB, *et al*. The role of myeloid cells in the promotion of tumour angiogenesis. *Nat Rev Cancer* 2008;8:618–31.
4 Petrova V, Annicchiarico-Petruzzelli M, Melino G, *et al*. The hypoxic tumour microenvironment. *Oncogenesis* 2018;7:10.
5 Doedens AL, Stockmann C, Rubinstein MP, *et al*. Macrophage expression of hypoxia-inducible factor-1 alpha suppresses T-cell function and promotes tumor progression. *Cancer Res* 2010;70:7465–75.
6 Jain RK. Antiangiogenesis strategies revisited: from starving tumors to alleviating hypoxia. *Cancer Cell* 2014;26:605–22.
7 Whatcott CJ, Han H, Von Hoff DD. Orchestrating the tumor microenvironment to improve survival for patients with pancreatic cancer: normalization, not destruction. *Cancer J* 2015;21:299–306.
8 Kahn BM, Lucas A, Alur RG, *et al*. The vascular landscape of human cancer. *J Clin Invest* 2021;131:e136655.
9 Folkman J. Tumor angiogenesis: therapeutic implications. *N Engl J Med* 1971;285:1182–6.
10 Ren S, Xiong X, You H, *et al*. The combination of immune checkpoint blockade and angiogenesis inhibitors in the treatment of advanced non-small cell lung cancer. *Front Immunol* 2021;12:689132.
11 Ko JS, Zea AH, Rini BI, *et al*. Sunitinib mediates reversal of myeloid-derived suppressor cell accumulation in renal cell carcinoma patients. *Clin Cancer Res* 2009;15:2148–57.

12 Falcon BL, Chintharlapalli S, Uhlik MT, *et al*. Antagonist antibodies to vascular endothelial growth factor receptor 2 (VEGFR-2) as anti-angiogenic agents. *Pharmacol Ther* 2016;164:204–25.
13 Goel HL, Mercurio AM. Vegf targets the tumour cell. *Nat Rev Cancer* 2013;13:871–82.
14 Chatterjee S, Heukamp LC, Siobal M, *et al*. Tumor VEGF: VEGFR2 autocrine feed-forward loop triggers angiogenesis in lung cancer. *J Clin Invest* 2013;123:1732–40.
15 Ferrara N. Vascular endothelial growth factor: basic science and clinical progress. *Endocr Rev* 2004;25:581–611.
16 Gille H, Kowalski J, Li B, *et al*. Analysis of biological effects and signaling properties of Flt-1 (VEGFR-1) and KDR (VEGFR-2). A reassessment using novel receptor-specific vascular endothelial growth factor mutants. *J Biol Chem* 2001;276:3222–30.
17 Meyer M, Clauss M, Lepple-Wienhues A, *et al*. A novel vascular endothelial growth factor encoded by ORF virus, VEGF-E, mediates angiogenesis via signalling through VEGFR-2 (KDR) but not VEGFR-1 (flt-1) receptor tyrosine kinases. *EMBO J* 1999;18:363–74.
18 Fukumura D, Kloepper J, Amoozgar Z, *et al*. Enhancing cancer immunotherapy using antiangiogenics: opportunities and challenges. *Nat Rev Clin Oncol* 2018;15:325–40.
19 Eelen G, Treps L, Li X, *et al*. Basic and therapeutic aspects of angiogenesis updated. *Circ Res* 2020;127:310–29.
20 Saltz LB, Clarke S, Díaz-Rubio E, *et al*. Bevacizumab in combination with oxaliplatin-based chemotherapy as first-line therapy in metastatic colorectal cancer: a randomized phase III study. *J Clin Oncol* 2008;26:2013–9.
21 Wallin JJ, Bendell JC, Funke R, *et al*. Atezolizumab in combination with bevacizumab enhances antigen-specific T-cell migration in metastatic renal cell carcinoma. *Nat Commun* 2016;7:12624.
22 Finn RS, Qin S, Ikeda M, *et al*. Atezolizumab plus bevacizumab in unresectable hepatocellular carcinoma. *N Engl J Med* 2020;382:1894–905.
23 Park JA, Santich BH, Xu H, *et al*. Potent ex vivo armed T cells using recombinant bispecific antibodies for adoptive immunotherapy with reduced cytokine release. *J Immunother Cancer* 2021;9:e002222.
24 Park JA, Cheung N-KV. Gd2 or HER2 targeting T cell engaging bispecific antibodies to treat osteosarcoma. *J Hematol Oncol* 2020;13:172.
25 Xu H, Cheng M, Guo H, *et al*. Retargeting T cells to GD2 pentasaccharide on human tumors using bispecific humanized antibody. *Cancer Immunol Res* 2015;3:266–77.
26 Lopez-Albaitero A, Xu H, Guo H, *et al*. Overcoming resistance to HER2-targeted therapy with a novel HER2/CD3 bispecific antibody. *Oncoimmunology* 2017;6:e1267891.
27 Orcutt KD, Ackerman ME, Cieslewicz M, *et al*. A modular igg-scfv bispecific antibody topology. *Protein Eng Des Sel* 2010;23:221–8.
28 Reikofski J, Tao BY. Polymerase chain reaction (PCR) techniques for site-directed mutagenesis. *Biotechnol Adv* 1992;10:535–47.
29 Yu L, Wu X, Cheng Z, *et al*. Interaction between bevacizumab and murine VEGF-A: a reassessment. *Invest Ophthalmol Vis Sci* 2008;49:522–7.
30 Bocci G, Man S, Green SK, *et al*. Increased plasma vascular endothelial growth factor (VEGF) as a surrogate marker for optimal therapeutic dosing of VEGF receptor-2 monoclonal antibodies. *Cancer Res* 2004;64:6616–25.
31 King C, Hristova K. Direct measurements of VEGF-VEGFR2 binding affinities reveal the coupling between ligand binding and receptor dimerization. *J Biol Chem* 2019;294:9064–75.
32 Mujagic E, Gianni-Barrera R, Trani M, *et al*. Induction of aberrant vascular growth, but not of normal angiogenesis, by cell-based expression of different doses of human and mouse VEGF is species-dependent. *Hum Gene Ther Methods* 2013;24:28–37.
33 Park JA, Wang L, Cheung N-KV. Modulating tumor infiltrating myeloid cells to enhance bispecific antibody-driven T cell infiltration and anti-tumor response. *J Hematol Oncol* 2021;14:142.
34 Ager A, May MJ. Understanding high endothelial venules: lessons for cancer immunology. *Oncoimmunology* 2015;4:e1008791.
35 Vella G, Guelfi S, Bergers G. High endothelial venules: a vascular perspective on tertiary lymphoid structures in cancer. *Front Immunol* 2021;12:736670.
36 Hurwitz H, Fehrenbacher L, Novotny W, *et al*. Bevacizumab plus irinotecan, fluorouracil, and leucovorin for metastatic colorectal cancer. *N Engl J Med* 2004;350:2335–42.
37 McDermott DF, Huseni MA, Atkins MB, *et al*. Clinical activity and molecular correlates of response to atezolizumab alone or in combination with bevacizumab versus sunitinib in renal cell carcinoma. *Nat Med* 2018;24:749–57.
38 Hicklin DJ, Ellis LM. Role of the vascular endothelial growth factor pathway in tumor growth and angiogenesis. *J Clin Oncol* 2005;23:1011–27.
39 Liang W-C, Wu X, Peale FV, *et al*. Cross-Species vascular endothelial growth factor (VEGF) -blocking antibodies completely inhibit the growth of human tumor xenografts and measure the contribution of stromal VEGF. *J Biol Chem* 2006;281:951–61.
40 Chen Y, Wiesmann C, Fuh G, *et al*. Selection and analysis of an optimized anti-VEGF antibody: crystal structure of an affinity-matured Fab in complex with antigen. *J Mol Biol* 1999;293:865–81.
41 Muller YA, Li B, Christinger HW, *et al*. Vascular endothelial growth factor: crystal structure and functional mapping of the kinase domain receptor binding site. *Proc Natl Acad Sci U S A* 1997;94:7192–7.
42 Neuchrist C, Erovic BM, Handisurya A, *et al*. Vascular endothelial growth factor receptor 2 (VEGFR2) expression in squamous cell carcinomas of the head and neck. *Laryngoscope* 2001;111:1834–41.
43 Girard JP, Springer TA. High endothelial venules (hevs): specialized endothelium for lymphocyte migration. *Immunol Today* 1995;16:449–57.
44 von Andrian UH, Mempel TR. Homing and cellular traffic in lymph nodes. *Nat Rev Immunol* 2003;3:867–78.
45 Rosen SD. Ligands for L-selectin: homing, inflammation, and beyond. *Annu Rev Immunol* 2004;22:129–56.
46 Hayasaka H, Taniguchi K, Fukai S, *et al*. Neogenesis and development of the high endothelial venules that mediate lymphocyte trafficking. *Cancer Sci* 2010;101:2302–8.
47 Martinet L, Garrido I, Filleron T, *et al*. Human solid tumors contain high endothelial venules: association with T- and B-lymphocyte infiltration and favorable prognosis in breast cancer. *Cancer Res* 2011;71:5678–87.
48 Girard J-P, Moussion C, Förster R. HEVs, lymphatics and homeostatic immune cell trafficking in lymph nodes. *Nat Rev Immunol* 2012;12:762–73.
49 Blanchard L, Girard JP. High endothelial venules (hevs) in immunity, inflammation and cancer. *Angiogenesis* 2021;24:719–53.
50 Allen E, Jabouille A, Rivera LB, *et al*. Combined antiangiogenic and anti-PD-L1 therapy stimulates tumor immunity through HEV formation. *Sci Transl Med* 2017;9:eaak9679.
51 Asrir A, Tardiveau C, Coudert J, *et al*. Tumor-associated high endothelial venules mediate lymphocyte entry into tumors and predict response to PD-1 plus CTLA-4 combination immunotherapy. *Cancer Cell* 2022;40:318–34.
52 Walker EJ, Su H, Shen F, *et al*. Bevacizumab attenuates VEGF-induced angiogenesis and vascular malformations in the adult mouse brain. *Stroke* 2012;43:1925–30.
53 Yang J, Yan J, Liu B. Targeting VEGF/VEGFR to modulate antitumor immunity. *Front Immunol* 2018;9:978.
54 Motz GT, Santoro SP, Wang LP, *et al*. Tumor endothelium FasL establishes a selective immune barrier promoting tolerance in tumors. *Nat Med* 2014;20:607–15.
55 Suzuki H, Onishi H, Wada J, *et al*. Vegfr2 is selectively expressed by foxp3high CD4+ Treg. *Eur J Immunol* 2010;40:197–203.
56 Elamin YY, Rafee S, Toomey S, *et al*. Immune effects of bevacizumab: killing two birds with one stone. *Cancer Microenviron* 2015;8:15–21.
57 Hu K, Olsen BR. Osteoblast-derived VEGF regulates osteoblast differentiation and bone formation during bone repair. *J Clin Invest* 2016;126:509–26.
58 Clere N, Renault S, Corre I. Endothelial-to-mesenchymal transition in cancer. *Front Cell Dev Biol* 2020;8:747.